CHEMISTRY & SUSTAINABILITY

CHEMSUSCHEM

ENERGY & MATERIALS

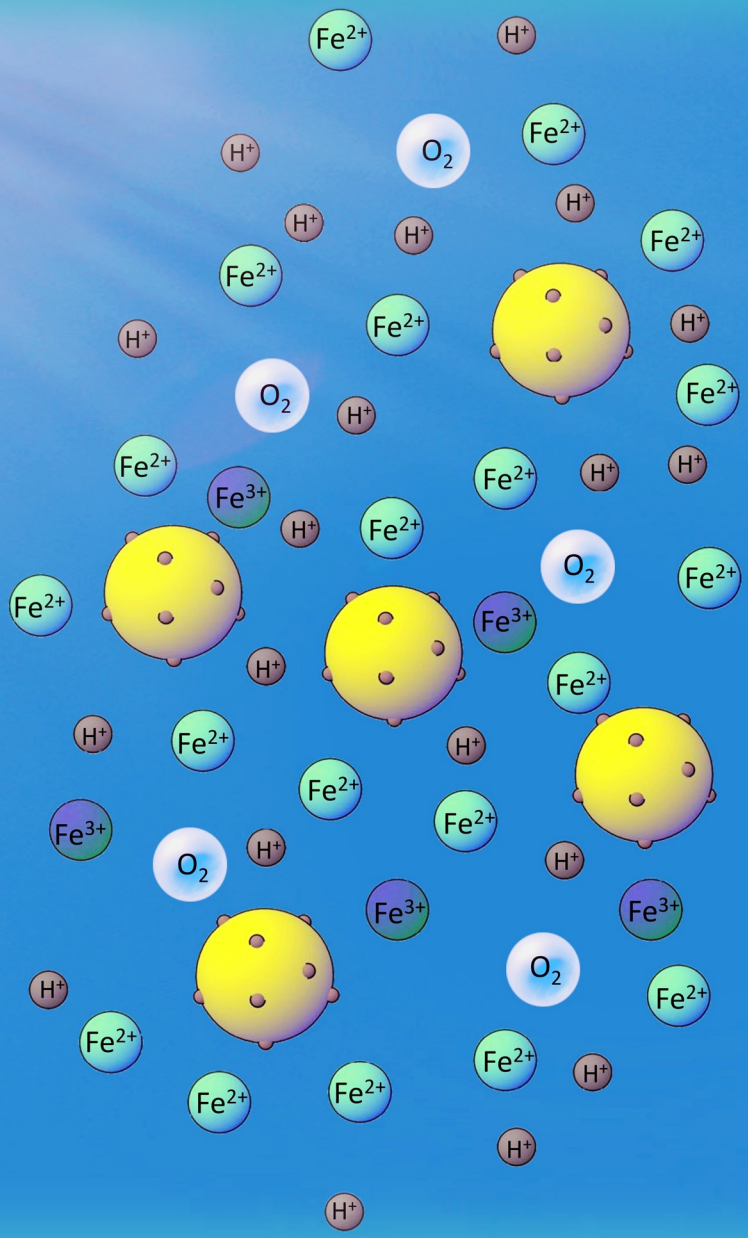

10/2017

Cover Picture:
Han et al.
Reliable Performance Characterization
of Mediated Photocatalytic Water-Splitting Half Reactions

A Journal of
ChemPubSoc Europe

WILEY-VCH

www.chemsuschem.org

ChemPubSoc Europe

DOI: 10.1002/cssc.201601901

CHEMSUSCHEM Full Papers

Reliable Performance Characterization of Mediated Photocatalytic Water-Splitting Half Reactions

Lihao Han,[a, b] Meng Lin,[a] and Sophia Haussener*[a]

Photocatalytic approaches using two sets of semiconductor particles and a pair of redox-shuttle mediators are considered as a safe and economic solution for solar water splitting. Here, accurate experimental characterization techniques for photocatalytic half reactions are reported, investigating the gas as well as the liquid products. The methods are exemplified utilizing photocatalytic titania particles in an iron-based aqueous electrolyte for effective oxygen evolution and mediator reduction reactions under illumination. Several product characterization methods, including an optical oxygen sensor, pressure sensor, gas chromatography, and UV/Vis spectroscopy are used and compared for accurate, high-resolution gas-products and mediator conversion measurements. Advantages of each technique are discussed. A high Faraday efficiency of 97.5 ± 2% is calculated and the reaction rate limits are investigated.

Introduction

Hydrogen fuel has attracted much attention as a versatile energy vector for a sustainable energy economy.[1,2] However, the majority of H_2 is currently produced from fossil fuels and therefore does not contribute to a transition towards a renewable and sustainable energy future. Various technologies to produce H_2 using renewable energy sources are possible. Efficient photoelectrochemical and photocatalytic solar-to-hydrogen (STH) conversion has the potential to become a cost-effective and scalable H_2 production approach with a significant impact on our energy economy.[3–12]

Photocatalytic water splitting in particle-slurry reactors is considered economically promising for the direct STH production.[13] These reactors can mimic natural photosynthesis of green plants following a Z-Scheme procedure, that is, utilizing one set of particles for the production of O_2 and another set of particles for the production of H_2. A mediator species shuttles the electrons from one particle type to the other. If the two sets of particles are separated by a semi-permeable membrane, this approach can provide a system that produces pure streams of H_2 and O_2 in spatially separated compartments. Compared with the panel array-based reactors (either fixed panels or tracking concentrator panels), the particle-slurry reactors have various advantages such as simplicity and flexibility in the reactor design and optimization, and potentially lower fuel cost.[5,14–16]

Accurate performance characterization is vital in the development of particle-slurry-based photocatalytic components and reactors. A challenge is the accuracy in the reaction-product measurements owing to relatively low efficiency of many photocatalytic particles. The amount and concentration of the generated H_2 and O_2 gases are very small in a lab-scale particle-slurry-based reactor compared with the large amount of O_2 in the atmosphere (ca. 0.1–5 vs. 20.95 vol%), and correspondingly difficult to detect. Furthermore, these reactors are based on suspended micro- or nanoparticles without the straightforward possibility of measuring the current densities or potentials, unlike in panel-based systems. Detecting the current and voltage in a particle-slurry-based reactor is impossible because a (photo-)cathode or (photo-)anode cannot be defined. As a result, crucial information for the analysis, characterization, and understanding of the system is missing. Generally, the 2:1 molar ratio of evolved H_2 to O_2 is reported as evidence of the conservation of charge and full charge-to-product conversion. However, no clear understanding of the kinetics of the different reactions or competition reactions, including side reactions and back reactions occurring simultaneously, can be gained from H_2 or O_2 measurements only.[17–19]

Here we present an accurate characterization methodology focusing not only on the quantification of the gas products but also the liquid products, to gain a better understanding of the various reactions occurring simultaneously in photocatalytic particle suspensions. We exemplify the approach on the O_2 evolving half reaction of the overall water-splitting reaction by utilizing commercially available rutile titania particles in suspension. The particles oxidize the water and reduce the mediator, which we chose to be Fe^{3+}. We investigate various techniques for the product characterization: for the gas products, we compare optical O_2 sensor, pressure sensor, and GC; for the

[a] Dr. L. Han, M. Lin, Dr. S. Haussener
Laboratory of Renewable Energy Science and Engineering
Swiss Federal Institute of Technology in Lausanne (EPFL)
Station 9, EPFL, 1015 Lausanne (Switzerland)
E-mail: sophia.haussener@epfl.ch

[b] Dr. L. Han
Current affiliation:
Joint Center for Artificial Photosynthesis
California Institute of Technology
Pasadena, California 91125 (United States)

Supporting Information for this article can be found under: http://dx.doi.org/10.1002/cssc.201601901.

liquid products, we use UV/Vis spectroscopy. We show how this approach can be used to quantify and compare the photocatalytic performance of particle suspensions proceeding under different operating conditions (varying mediator concentrations and particle concentrations) to provide evidence that transport limitations can significantly affect the measurement results.

Results and Discussion

Particle-slurry reactor design considerations

We follow the definition by James et al.:[5,13] A single-bed particle-suspension reactor in which the hydrogen evolution reaction (HER) and oxygen evolution reaction (OER) proceed on the surface of the same particle type (resulting in co-evolution of H_2 and O_2) is called a Type 1 reactor (Figure 1 a), and a dual-bed reactor in which the HER and OER proceed on different particle types in separated beds (allowing for spatially-separated generation of H_2 and O_2) is called a Type 2 reactor (Figure 1 b). However, conservation of charge requires a means of transporting electrons from the O_2-evolving particle type to the H_2-evolving particle type. This can be achieved by different approaches, for example, a mediator redox couple shuttling the electrons from one particle type to the other,[18,19] or a combination of mediator couple and wire requiring two additional electrochemical reactions.[17] Type 1 reactors potentially have higher STH efficiencies than Type 2 reactors because there are no additional electrochemical reactions with corresponding losses taking place and no mass-transport limitation of the redox-couple species are present.[5] However, considerable efforts are required to ensure that the operation of this system is safe and the products can be effectively separated and collected. The gas-separation step in the post-treatment for the gas-phase products increases the final cost of energy by introducing carrier gas and additional auxiliary equipment. The safety issues during the gas separation also require careful considerations.

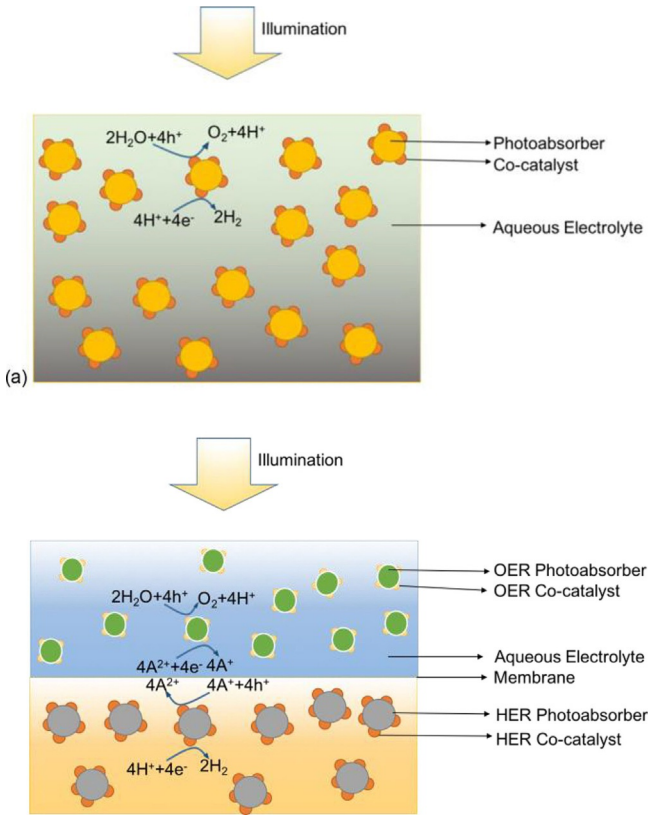

Figure 1. (a) An illustration of a Type 1 photocatalytic reactor in which HER and OER occur on the surface of the same semiconductor particle. (b) A Type 2 photocatalytic reactor in which HER and OER occur on the surface of different sets of particles. These particles are in the micrometer or nanometer scale.

Type 2 reactors can overcome this drawback and additionally allow for more flexibility in the use of photocatalytic materials because the OER and HER are proceeding on different particles, requiring different alignment of the valence and conduction bands. Moreover, Type 2 reactors are flexible in optimizing HER and OER independently, require no gas-mixture separation, and operate intrinsically safe. Furthermore, a top-bottom arrangement of the beds (in contrast to a side-by-side arrangement) in Type 2 provides the opportunity to more efficiently use the solar radiation, equivalent to a tandem dual-absorber approach. Typical photo-absorber materials are pure or modified semiconductors, such as TiO_2,[17–23] $TiSrO_3$,[15,24,25] WO_3,[26,27] TaON,[19,28–30] $BiVO_4$,[15] Cu_2O,[31] CoO,[32] and III–V group[33] and perovskite materials.[34–36] Major considerations in choosing a photo-absorber particles are: 1) the optical band gap, which should be suitable so that a large fraction of the solar spectrum can be utilized; 2) the band edge positions, which should be suitable to meet the thermodynamic requirement of the oxidation (OER and mediator oxidation) and reduction reactions (mediator reduction and HER); 3) corrosion residence in aqueous electrolyte; and iv) chemical activity and selectivity for efficient photocatalytic water-splitting reactions (OER, HER, mediator oxidation and reduction).[16] To facilitate a more efficient reaction, co-catalysts are sometimes coated onto the photo-absorber particles. The option of co-catalysts varies between metals (such as Pt[19,24,30,37,38] and Ru[25,39]), metal oxides (such as PtO_x,[28,29] RuO_2,[40–43] NiO_x,[44,45] and IrO_2[24]), and other chemical compounds or alloys (such as $RhCrO_x$,[46] Ni–Mo,[47] and Pt–Ru[48,49]). Materials commonly utilized as redox-shuttle couple are Fe^{3+}/Fe^{2+},[17] I^-/IO_3^-,[19] NO_3^-/NO_2^-,[50] $[Co(bpy)_3]^{3+/2+}$, and $[Co(phen)_3]^{3+/2+}$.[51]

Here, we investigate one bed of a dual-bed reactor (Type 2) utilized for overall water splitting, namely the OER and mediator reduction side. We chose rutile TiO_2 as a model material to exemplify the measurement methodology. Titania was chosen owing to its effective UV photon absorption, aligned band-edge position for OER, and photocatalytic activity. Besides, titania represents one of the most challenging scenarios for our method because its O_2 production rate is low (a few hundred µmol O_2 per hour and g TiO_2) owing to its relatively large band gap (ca. 3.2 eV). The OER system used here can be seen as a general example of a particle system relevant in a Z-Scheme photocatalytic process with a dual-bed reactor used for water splitting or CO_2 reduction. Furthermore, even in a single-bed

reactor type, the tiny amount of H_2 can be easily determined by subtracting the produced O_2 amount from the total amount of product-gas mixture.

Methods and model system

Figure 2 illustrates the experimental batch reactor used to exemplify the product characterization methods for mediated

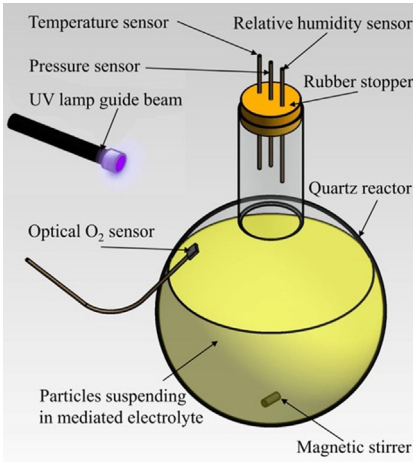

Figure 2. A sketch illustration of the experimental setup. The OER occurs in a sealed quartz flask containing rutile TiO_2 particles (100 mg) in $FeCl_3$ aqueous solution (50 mL). Various gas-product characterization techniques including the optical O_2 sensor and the pressure sensor are indicated. The quartz reactor diameter is approximately 5 cm.

photocatalytic reactors. Rutile TiO_2 particles (100 mg) were suspended in 4 mM $FeCl_3$ aqueous solution (50 mL) in a quartz flask with a stirring magnet (details described in the Experimental Section). During continuous illumination by a UV lamp, electron and hole pairs were generated in the rutile TiO_2 particles when absorbing photons. The ferric ions were gradually reduced into ferrous ions, and the water was oxidized into O_2 [Eqs. (1)–(3)]. This reaction is used as an example owing to the high photocatalytic activity of the TiO_2 particle towards OER and the relatively simple chemical reaction steps.

$$4\,h\nu \rightarrow 4\,e^- + 4\,h^+ \quad (1)$$

$$4\,Fe^{3+} + 4\,e^- \rightarrow 4\,Fe^{2+} \quad \text{(in aqueous electrolyte)} \quad (2)$$

$$2\,H_2O + 4\,h^+ \rightarrow 4\,H^+ + O_2\uparrow \quad \text{(in aqueous electrolyte)} \quad (3)$$

Optical sensor for O_2 characterization

An optical O_2 sensor PreSens Fibox3 was introduced to monitor the O_2 concertation in the gas-phase product during the solar water-splitting reactions. The principle of measurement for the optical O_2 sensor is based on the effect of dynamic luminescence quenching by molecular O_2. The collision between the luminophore in its excited state and the quencher (O_2) results in radiationless deactivation and is called collisional or dynamic quenching. After collision, energy transfer occurs from the excited indicator molecule to O_2, which consequently is transferred from its ground state (triplet state) to its excited singlet state. As a result, the indicator molecule does not emit luminescence, and the measurable luminescence signal decreases. The advantage of the optical sensors is that they can be physically separated from the measuring system, allowing noninvasive measurements. This method can measure with a relatively high frequency of two data points per second (2 Hz) with high repeatability. An accurate calibration is required, for which we used humid air (20.95% of which is O_2) and pure nitrogen (0% of which is O_2). The measurement error owing to pre-calibration is estimated to be ±2%.

The black curve in Figure 3 shows a typical O_2 measurement with the O_2 sensor with a temporal resolution of 1 Hz for the

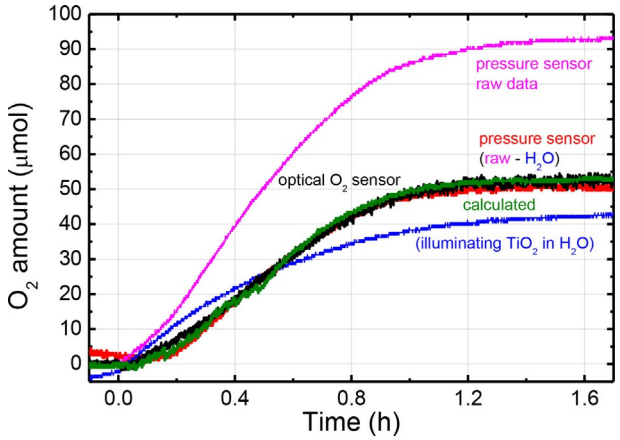

Figure 3. In situ O_2 generation characterization using an optical O_2 sensor (black curve), and an in-house developed pressure sensor (green and red curves). The purple curve shows the raw data measured by the pressure sensor before calibration. The green curve shows the calculated curve accounting for the water vapor, ideal gas law, and O_2 solubility variation introduced by heating. The blue curve shows the heating effects of the rutile TiO_2 in water under the same conditions as the photocatalytic reaction but without mediator. The red curve is the sample O_2 evolution amount by subtracting the data in the blue curve from the purple curve. The sealed quartz flask contained rutile TiO_2 (100 mg) in 4 mM $FeCl_3$ mediator solution (50 mL) before illumination by the focused UV beam from an OminiCure series 1000 lamp at a distance of approximately 3 cm.

rutile TiO_2 in 4 mM $FeCl_3$. The electrolyte was purged with pure N_2 gas for 10–15 min before sealing the headspace of the quartz flask. The amount of O_2 was determined by measuring the O_2 concentration in the headspace and typically varied between 0.0 and approximately 5.5%. The O_2 amount was continuously increasing in the first hour of illumination and saturated afterwards because the Fe^{3+} was almost completely converted into Fe^{2+}.

Pressure sensor for gas-product characterization

An in-house developed differential pressure-sensor device with an ASDX005D44R-A chip from the First Sensor company was

utilized to measure the increase in pressure in the headspace of the sealed glass flask. The pressure in the flask increases upon illumination from atmospheric pressure, p_{ini}, to the final measured pressure, according to the amount of evolved gas. The pressure sensor has a resolution as high as 1024 Hz and a sensitivity of approximately 5 μbar. This method is repeatable as long as the atmosphere pressure does not significantly vary during the measurement (i.e., stays within ±3%).

This method needs to be carefully calibrated because the measured pressure significantly depends on the operating conditions. Particularly, four physical effects affect the measurement: 1) water vapor pressure changes with temperature; 2) thermal expansion of the gases in the sealed flask; 3) O_2 release from the aqueous electrolyte owing to heating; and 4) O_2 release owing to salinity change.

During the 100 min intensive UV-light illumination, TiO_2 particles absorb photons and gradually heat the aqueous electrolyte from approximately 22 °C (T_{ini}) to 28 °C (measured by an in situ temperature sensor inserted in the headspace of the sealed flask). The water evaporation increases with temperature (relevant T range ca. 22–28 °C) and relative humidity (RH; relevant RH range ca. 70–100%), increasing the pressure in the flask even though no additional O_2 is generated. To correct for this effect, the amount of evaporated water was calculated according to Equation (4) using the psychrometric chart for the mixture of water vapor and air; 4 mM $FeCl_3$ solution was considered as pure water because the weight ratio of $FeCl_3/H_2O$ is as small as approximately 0.032 g:50 g).[52] The RH was measured by an in situ RH sensor inserted in the headspace of the sealed flask.

$$n_{vapor} = V_{voidspace} p_{ini} R^{-1} T_{ini}^{-1} \times M_{air} \times 10^{-3} \left[\omega(T_p, p_p, RH_p) - \omega(T_{ini}, p_{ini}, RH_{ini})\right] \quad (4)$$

n_{vapor} is the vapor amount [μmol], $V_{voidspace}$ is the sum of the flask's headspace and the tube volume connected to the sensor [mL], R is the ideal gas constant [J mol^{-1} K^{-1}], M_{air} is the molar mass of air [g mol^{-1}], and ω is the humidity ratio [kg_{vapor} kg_{air}^{-1}] depending on T, p, and RH at present state (subscript p) and initial state (subscript ini). We treated the gas mixture as an ideal gas to correct for the thermal expansion of the gas ($n_{thermal\ expansion} = n_{measured} T_p T_{ini}^{-1}$).

The reduction of the O_2 solubility in the water (i.e., aqueous electrolyte) with increasing temperature is accounted for by calculating the amount of released O_2 within increasing temperature, according to the solubility of O_2 in water at each specific temperature [Eqs. (5) and (6)]:[52–54]

$$c_{O_2,T} = 1.443 \times 10^{-7} T^4 - 6.57 \times 10^{-5} T^3 + 6.925 \times 10^{-3} T^2 - 0.382T + 14.42 \quad (5)$$

$$n_{O_2} = V_{electrolyte} M_{O_2}^{-1} \times (c_{O_2,T_{ini}} - c_{O_2,T_p}) \quad (6)$$

in which $c_{O_2,T}$ is the temperature-dependent O_2 solubility in water [mg L^{-1}], $V_{electrolyte}$ is the volume of the electrolyte [mL], M_{O_2} is the molar mass of O_2 [g mol^{-1}], and n_{O_2} is the enhanced amount of O_2 owing to the solubility variation [μmol].

Moreover, we considered the temperature-dependent salinity variation, known as salting-out effect.[55,56] With the evaporation of water, the Cl^- concentration in the aqueous electrolyte changes, resulting in different solubility values of O_2 in water. This effect was estimated to be minor, that is, a ΔT of 4 K at atmospheric pressure resulted in approximately 2×10^{-12} mol O_2 release from 50 mL aqueous solution containing [Cl^-] as small as 4 mM, and can always be ignored.[55,57,58]

The corrected pressure measurement can then be estimated according to Equation (7):

$$n_{corrected} = n_{measured} T_p T_{ini}^{-1} - n_{vapor} - n_{O_2} \quad (7)$$

The overall measurement error on the measured pressure data is estimated to be ±5%. The green curve in Figure 3 shows the O_2 amount measured by the pressure sensor (raw data in purple), which is corrected for the above-mentioned temperature effects. The corrected pressure reading compares well to the O_2 data measured by the optical O_2 sensor (maximum variation is ≈5% at 1.22 and 1.63 h). For confirmation, a control experiment was conducted in which pure water with dispersed TiO_2 particles (same particles and concentration) was exposed to the UV irradiation and therefore heated to the same temperature at the same rates as in the photocatalytic experiment. This experiment isolates the temperature effect, and its pressure reading (blue curve) can be subtracted from the raw data (purple curve, true photocatalytic experiment). A similar correction as the analytical one introduced above was obtained, providing further evidence that the introduced analytical correction [Eq. (7)] accurately describes the actual O_2 evolution.

This experiment underlines the accuracy of the pressure-based gas-production measurement method. The accuracy, quantified by a mean deviation of the estimated/corrected data and the measured oxygen data (by the oxygen sensor), is 2.13 μmol for the calculated data (green curve) and 3.59 μmol for the corrected pressure data (red curve). It can be equally used for the measurement of other product gases such as H_2, utilizing the same temperature correction (shown for H_2 production in the Supporting Information). In addition to the accuracy of the measurement of small amounts of evolved O_2, the pressure sensor also exhibits a very high frequency (up to 1 ms resolution with our sensor). This high-resolution product-gas measurement allows for a more detailed understanding of the process; for instance, the unsteady effects of the reactions are easier to reveal. The O_2 solubility in the aqueous electrolyte with rising temperature should also be considered during product characterization with the optical O_2 sensor. The manufacturer of the PreSens Fibox3 sensor has already considered this effect during calibration and no additional correction is needed.

Gas chromatography for gas-product characterization

GC is a technique for separating and analyzing gas compounds without decomposition according to the differences of the boiling points (or vapor pressure) in the gas mixture. It is gen-

erally used for identifying a gas-phase compound, testing the purity of a particular substance, separating various types of components from the gas mixture, and accurately quantifying the concentration of specific sample gases.[59,60] GC is one of the most accurate and repeatable techniques for measuring the concentration of gases because the area value can be accurately integrated from the specific peak in the chromatogram. The disadvantages of GC are that the result is sensitive to calibration errors and that the calibration step is relatively complex and expensive. Besides, the time-resolution of GC measurements is in the minute range, hundred to thousand times slower than the sensor methods. Consequently, information on unsteady behavior at the initial step of the process is not accessible.

We used a Shimadzu GC-8A with a thermal conductivity detector (TCD) and MS-5A columns filled with argon as the carrier gas in the closed cycle for the O_2 characterization in the same photocatalytic reaction using rutile TiO_2 and $FeCl_3$ aqueous electrolyte. We confirmed that the evolved gas is pure O_2 and the saturated amount is approximately 50 μmol, which is in accordance with the amounts obtained by the optical O_2 sensor and the pressure sensor under the same experimental conditions. The GC data have a low temporal resolution (ca. 30 min for one data point), that is, only two or three values can be measured in the complete reaction.

Liquid-product characterization

The recording of the concentration of the mediator is essential to study the side reaction or back reaction during the photocatalytic process. Two methods, ion chromatography (IC) and UV/Vis spectroscopy, are commonly utilized in practice.[61–64]

IC is a chromatography technique that separates ions and polar molecules based on their interaction with a resin, and consequently measures the concentrations of ionic species according to their affinity to the ion exchanger. The IC setups are capable to quantify the concentrations of major anions, including Cl^-, F^-, Br^-, NO_3^-, and SO_4^{2-}, and major cations including Li^+, Na^+, NH_4^+, K^+, Ca^{2+}, and Mg^{2+}, as well as some organic acids. The resolution of IC can be as high as parts-per-billion (ppb) range. However, we do not show the characterization results for the mediator concentrations in this OER because a standard IC setup cannot distinguish Fe^{2+} and Fe^{3+} ions individually but only their total amount.[65]

In this work, we use UV/Vis spectroscopy (Varian setup Cary 100 Bio) to measure the absorption or reflectance in the UV/Vis spectral region. This technique is fast (1–2 min for one measurement) and easy to use. Some salts (such as NH_4Cl, $FeCl_3$, $FeCl_2$, Na_2CO_3) can hydrolyze in aqueous solution, and therefore their concentrations cannot be easily and directly measured. Thus, a colorimetry technique is utilized to complex the sample ions.[17,66] For example, the mediator couple Fe^{3+}/Fe^{2+} used here can be complexed by a KSCN solution and a TPTZ (2,4,6-tripyridyl-*s*-triazine) solution by forming red and blue complex solutions [$Fe(SCN)(H_2O)_5^{2+}$ and $Fe(TPTZ)_2^{2+}$], respectively.[66,67] We periodically siphoned off 10 μL of the electrolyte from the reactor, diluted it with deionized water, and

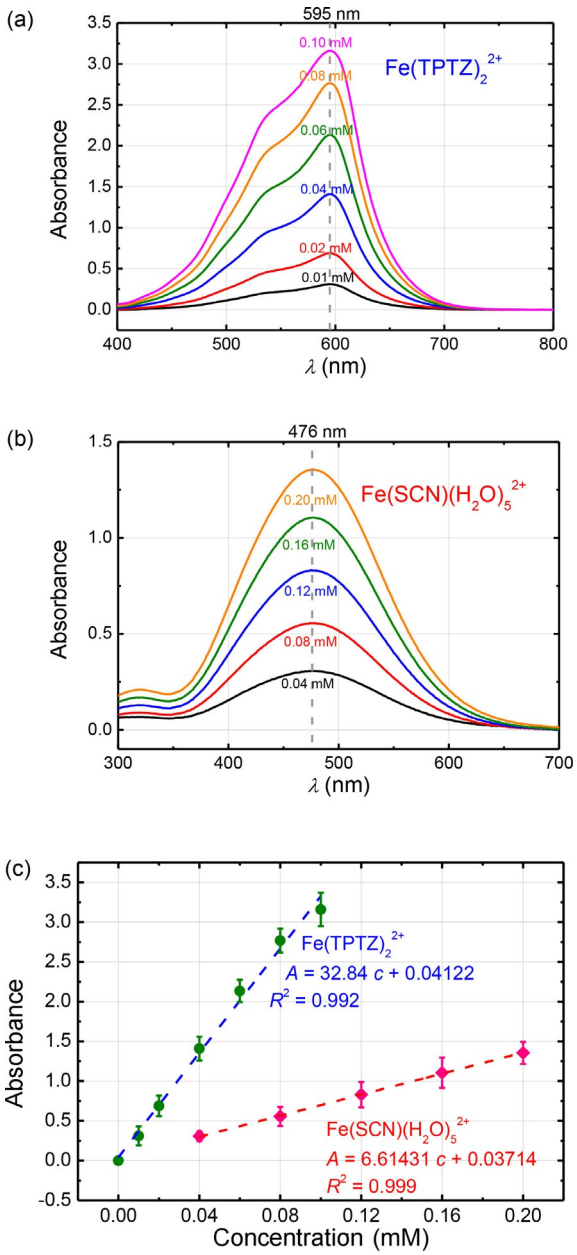

Figure 4. (a) UV/Vis absorption spectrum of $Fe(TPTZ)_2^{2+}$ solution with known concentration. (b) UV/Vis absorption spectrum of $Fe(SCN)(H_2O)_5^{2+}$ solution with known concentration. (c) Absorption versus Fe^{2+} (blue dashed curve) concentration and Fe^{3+} (red dashed curve) concentration analysis using the Beer–Lambert law.

then used it to determine the mediator concentration by colorimetry, as described below. The complexing of TPTZ with Fe^{2+} and of SCN^- ligands with Fe^{3+} should not be performed directly inside the flask because it influences the redox activity of the Fe^{2+}/Fe^{3+} couple.

Figure 4a shows the measured UV/Vis absorption of the $Fe(TPTZ)_2^{2+}$ solution with known concentration. This compound, even at low concentrations, has an intensive peak at 595 nm.

The Beer–Lambert law [Eq. (8)]

$$A = -\log_{10}(I_0/I) = \varepsilon Lc \quad (8)$$

is used to determine the mediator concentration in the aqueous electrolyte. A is the measured absorbance, I_0 is the initial light intensity, I is the transmitted light intensity, ε is the wavelength-dependent molar absorptivity coefficient [$M^{-1}\,cm^{-1}$], L is the path length, and c is the sample concentration. By analyzing the absorption intensities at 595 nm in Figure 4a, a linear curve is fitted, as plotted by the blue dashed line in Figure 4c. The concentration of Fe^{2+} [mM] is consequently determined according to Equation (9):

$$c = (A - 0.04122)/32.84 \ [\text{root mean square (RMS)} = 0.992] \quad (9)$$

The Fe^{3+} is complexed by KSCN, and the UV/Vis spectrum of the red $Fe(SCN)(H_2O)_5^{2+}$ solution is plotted in Figure 4b. The peak intensity of this component at 476 nm is linearly fitted as shown by the red dashed line in Figure 4c,[67] and the concentration of Fe^{3+} [mM] is determined by the Beer–Lambert law according to Equation (10):

$$c = (A - 0.03714)/6.61431 \ (\text{RMS} = 0.999) \quad (10)$$

Characterization of the half reaction

Utilizing all tools introduced before, we show the complete characterization of the water-splitting half reaction (OER) in a slurry of rutile TiO_2 particles (100 mg) in a 4 mM $FeCl_3$ mediator solution (Figure 5a). The molar amounts of Fe^{3+} and Fe^{2+} are shown by the green squares and red dots, respectively, and the evolved O_2 by the blue curve. The molar amount of Fe^{3+} gradually decreases from the initial 200 μmol to almost 0 after 1 h. The molar amount of Fe^{2+} gradually increases during the reaction from 0 to 189 μmol after 1 h. The sum of the mediator couple amounts ($Fe^{2+} + Fe^{3+}$) is indicated by the black triangles, which is close to the initial 200 μmol of Fe^{3+}, regardless of small measurement errors introduced by the UV/Vis spectroscopy analysis. We can utilize the in situ measurement of the generated O_2 and Fe^{2+} to determine the Faraday efficiency of the OER, assuming that the OER is favorable on rutile TiO_2,[17] no impurities in the aqueous electrolyte are reduced, and mass-transport limits equally affect all participating reactants and ions. The molar ratio of Fe^{2+} and O_2 is approximately 3.92:1 after 2 h illumination, which is very close to the theoretical 4:1 ratio expected according to Equations (2) and (3). Assuming that every electron is used for the reduction of the mediator, the fraction of the molar ratios can be used to estimate the Faraday efficiency of the OER. The Faraday efficiency of the OER is calculated to be 97.5 ± 2%. Under these conditions, the average O_2 evolution rate in this system is 67 μmol h^{-1} in the first 40 min and gradually slows afterwards owing to the decrease of the Fe^{3+} concentration as local mass-transport limitations start to dominate the behavior. Consequently, the time intervals for the determination of the reaction rate need to be carefully chosen. The average OER rate within the first 10 min is 46 μmol h^{-1}, within the first 40 min 78 μmol h^{-1}, and within the first hour 48 μmol h^{-1}. The instantaneous OER rate is calculated based on the blue curve in Figure 5a and plotted in Figure 5b. After 14 min illumination, the O_2 production rate reaches its maximum of 112 μmol h^{-1}. The concentration of Fe^{3+} in the aqueous electrolyte decreases by 30% of the initial value (calculated based on the green curve in Figure 5a); therefore, the availability of the mediator ion limits the continuous enhancement of the O_2 evolution rate.

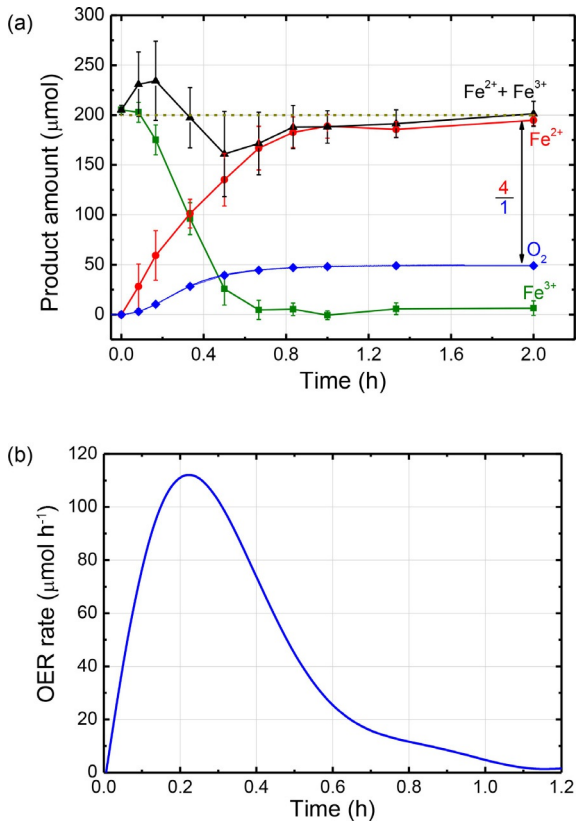

Figure 5. (a) Mediator-ion concentration determined by UV/Vis spectroscopy. When the TiO_2 particles were illuminated by a UV lamp, the water was gradually oxidized into O_2 (blue curve, obtained by the optical O_2 sensor measurements), whereas the ferric ions (green squares: Fe^{3+} amount in 50 mL H_2O) were gradually deoxidized into ferrous ions (red dots: Fe^{2+} amount in 50 mL H_2O). The sum of the mediator couple amounts is indicated by the black triangles. (b) Calculated instantaneous O_2 evolution rate during the photocatalytic reaction.

We investigated the water-splitting half reaction (OER) in batch configuration utilizing different operating conditions to obtain a detailed insight into the transport limitations in such a batch-type reactor. The concentration of TiO_2 photocatalysts was varied between 2 g L^{-1} (100 mg in 50 mL solution) and 8 g L^{-1} (400 mg in 50 mL solution), and the concentration of the initial Fe^{3+} mediator was varied between 4 mM (200 μmol in 50 mL solution) and 8 mM (400 μmol in 50 mL solution), as summarized in Table 1.

All conditions eventually result in full mediator-species conversion (Figure 6a); however, the OER rates are significantly dif-

Table 1. Experimental parameters for various OER in 50 mL aqueous electrolyte containing rutile TiO_2 particles as photocatalyst and Fe^{3+} as mediator.

Experiment	TiO_2 [g L^{-1}]	$FeCl_3$ [mM]	OER rate in the first 40 min [μmol h^{-1}]	OER rate normalized by the molar amount of $FeCl_3$ in the first 40 min [μmol $μmol_{FeCl_3}^{-1}$ h^{-1}]
Condition 1	2	4	65	0.325
Condition 2	8	4	61	0.305
Condition 3	2	8	25	0.063
Condition 4	8	8	55	0.138

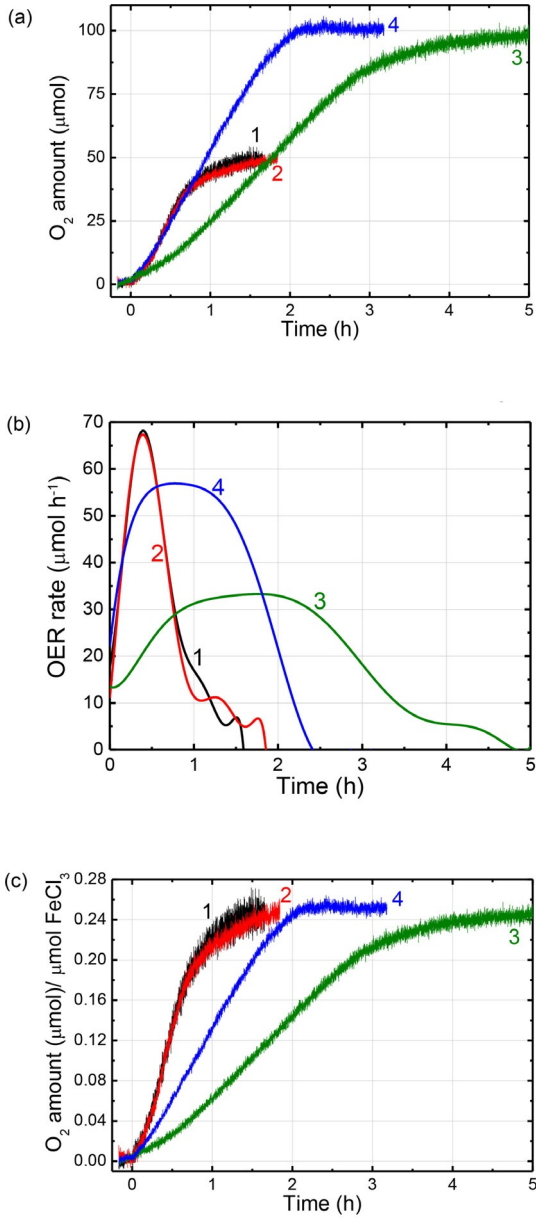

Figure 6. Reaction rate limitation study investigating varying amounts of TiO_2 photocatalyst and the Fe^{3+} mediator concentration. (a) In situ O_2 amount monitoring during the reaction. (b) Calculated instantaneous O_2 evolution rate during the photocatalytic reactions under four conditions. (c) O_2 amount normalized by the mediator amount. The quartz flask contains aqueous solution (50 mL) with 4 or 8 mM $FeCl_3$, and rutile TiO_2 powder (100 or 400 mg) with a magnetic stirring bar. Condition 1: 2 g_{TiO2} L^{-1} and 4 mM $FeCl_3$; Condition 2: 8 g_{TiO2} L^{-1} and 4 mM $FeCl_3$; Condition 3: 2 g_{TiO2} L^{-1} and 8 mM $FeCl_3$; and Condition 4: 8 g_{TiO2} L^{-1} and 8 mM $FeCl_3$. They are illuminated by an OminiCure series 1000 UV lamp from Technicia at a distance of approximately 3 cm.

ferent. The OER rates vary between 65 μmol h^{-1} (within ca. 3% variation compared to the same experiment shown in Figure 5), 61, 25, and 55 μmol h^{-1} for experimental Conditions 1–4, respectively (Table 1). More TiO_2 photocatalysts absorb more radiation and generate more electron-hole pairs, leading to faster OER rates as long as sufficient mediator species are available in the aqueous electrolyte, as shown by the comparison between Conditions 4 and 3 (ca. 2.2 times faster in the initial 40 min). However, the amount of photocatalyst is not limiting if the mediator concentration is sufficiently small, as observed when comparing Conditions 2 and 1 (similar rates). The reaction rate is limited by other factors such as mass transport or radiation absorption. The instantaneous OER rates under the four conditions are calculated based on Figure 6a and plotted in Figure 6b.

Figure 6c shows the evolved amount of O_2 normalized by the molar amount of $FeCl_3$ mediator. As the illumination continues, the normalized amount of O_2 per μmol $FeCl_3$ in these four experiments reaches almost the same value (0.26), indicating that the Faraday efficiencies of these reactions are similar and close to 100%. Because the $FeCl_3$ solution also absorbs in the UV range of the spectrum, the TiO_2 particles can in principle absorb more UV photons in a less concentrated solution; therefore, the reaction rate of Condition 1 is faster than that of Condition 3. This argument also holds when comparing the reaction rates of Condition 2 and Condition 4, and can only be concluded if the mediator concentration is normalized. The availability of the mediator in the batch system is affecting the normalized rate, generally reducing the rate with larger mediator concentration. This results from the limitation in the mass transport of the Fe^{3+} ions.

Conclusions

In this paper, several direct and indirect characterization methods, including optical O_2 sensor, pressure sensor, GC, and UV/Vis spectroscopy were demonstrated for a model half reaction of the solar-driven water-splitting reaction using semiconductor particles and mediators as redox shuttles. Advantages and bottlenecks of each technique were discussed. A high Faraday efficiency of 97.5±2% was estimated by measuring the evolved O_2 amount and mediator product amount. The limitation of the photocatalytic reaction rate was investigated by varying the concentrations of particles and mediator, respectively. More TiO_2 photocatalysts absorb more radiation and generate more electron-hole pairs, leading to faster OER rates as long as sufficient mediator species are available in the aque-

ous electrolyte. This article demonstrates high-resolution characterization methods for the gas-phase and liquid-phase product measurement in a photocatalytic reactor with mediators, providing reliable tools to study and characterize the photocatalytic reactions and their mechanism.

Experimental Section

In our standard photocatalytic reaction, as-purchased rutile TiO_2 particles (100 mg, Alfa Aesar, 99.8%, 0.9–1.6 micro) were suspended in 4 mM $FeCl_3$ aqueous solution (50 mL, Sigma–Aldrich, $\geq$99.99% anhydrous powder) in a quartz flask with a stirring magnet. This quartz flask, purchased from the Bluewin Glass Technology company in Switzerland, had a total sealed volume of 74 mL and was transparent in the spectral range of 260–4200 nm (specifically, >93% transparency in the range of 320–2500 nm). This flask was sealed by a tight rubber stopper using Apiezon wax W40 and silica grease, and was purged by bubbling pure N_2 through the aqueous electrolyte (freeze–pump–thaw cycles) for 20 min before the reaction started to remove dissolved O_2 in the electrolyte and the headspace of the flask. The reactor was then continuously illuminated by a UV lamp (OminiCure series 1000 from Technicia with an energy density of 13 W cm^{-2} in the wavelength range of 280–500 nm). The intensive UV light was focused using a guider beam. The evolved gas was characterized utilizing various techniques. An optical O_2 sensor PreSens Fibox3 was introduced to monitor the O_2 concertation in the gas-phase product. This sensor was calibrated in two environments: 0% O_2 concentration (pure N_2) and 20.95% O_2 concentration (atmospheric air at room temperature with 100% RH). An in-house developed differential pressure-sensor device using an ASDX005D44R-A chip from the First Sensor company was utilized to measure the increased pressure in the headspace of the sealed glass flask. The pressure reading was corrected for temperature effects, according to our description. A Shimadzu GC-8A with a TCD and MS-5A columns was employed for the gas-type and -amount characterization, and argon was injected as the carrier gas in the cycle. The aqueous electrolyte was investigated using UV/Vis spectroscopy with a Varian setup Cary 100 Bio.

Acknowledgements

This material is based upon work performed with the financial support of the starting grant of the Swiss National Science Foundation, as part of the SCOUTS project (grant #155876). We thank Dr. E. Amstad at EPFL for providing access to laboratory equipment and useful discussions. We thank D. Han and D. Perone for their support in the experimental investigations. We thank Dr. T. Hisatomi, Prof. Dr. K. Domen, and Dr. S. Chen for fruitful discussions and complementary measurement possibilities during L.H.'s visit at the University of Tokyo in Japan. Prof. Dr. H. A. Klok is acknowledged for providing access to the UV/Vis spectroscopy facility at EPFL.

Keywords: characterization · mediator · photocatalysis · titania · water splitting

[1] N. S. Lewis, D. G. Nocera, *Proc. Natl. Acad. Sci. USA* **2006**, *103*, 15729–15735.
[2] J. A. Turner, *Science* **2004**, *305*, 972–974.
[3] A. Nakamura, Y. Ota, K. Koike, Y. Hidaka, K. Nishioka, M. Sugiyama, K. Fujii, *Appl. Phys. Express* **2015**, *8*, 107101.
[4] F. F. Abdi, L. Han, A. H. M. Smets, M. Zeman, B. Dam, R. van de Krol, *Nat. Commun.* **2013**, *4*, 2195.
[5] B. A. Pinaud, J. D. Benck, L. C. Seitz, A. J. Forman, Z. B. Chen, T. G. Deutsch, B. D. James, K. N. Baum, G. N. Baum, S. Ardo, H. L. Wang, E. Miller, T. F. Jaramillo, *Energy Environ. Sci.* **2013**, *6*, 1983–2002.
[6] L. Han, F. F. Abdi, P. Perez Rodriguez, B. Dam, R. van de Krol, M. Zeman, A. H. M. Smets, *Phys. Chem. Chem. Phys.* **2014**, *16*, 4220–4229.
[7] J. S. Luo, J. H. Im, M. T. Mayer, M. Schreier, M. K. Nazeeruddin, N. G. Park, S. D. Tilley, H. J. Fan, M. Grätzel, *Science* **2014**, *345*, 1593–1596.
[8] L. Han, F. F. Abdi, R. van de Krol, R. Liu, Z. Huang, H.-J. Lewerenz, B. Dam, M. Zeman, A. H. M. Smets, *ChemSusChem* **2014**, *7*, 2832–2838.
[9] G. Peharz, F. Dimroth, U. Wittstadt, *Int. J. Hydrogen Energy* **2007**, *32*, 3248–3252.
[10] L. Han, I. A. Digdaya, T. W. F. Buijs, F. F. Abdi, Z. Huang, R. Liu, B. Dam, M. Zeman, W. A. Smith, A. H. M. Smets, *J. Mater. Chem. A* **2015**, *3*, 4155–4162.
[11] S. Y. Reece, J. A. Hamel, K. Sung, T. D. Jarvi, A. J. Esswein, J. J. H. Pijpers, D. G. Nocera, *Science* **2011**, *334*, 645–648.
[12] I. A. Digdaya, L. H. Han, T. W. F. Buijs, M. Zeman, B. Dam, A. H. M. Smets, W. A. Smith, *Energy Environ. Sci.* **2015**, *8*, 1585–1593.
[13] B. D. James, G. N. Baum, J. Perez, K. N. Baum, Directed Technologies Inc., (US DOE Contract no. GS-10F-009J), Arlington, VA, **2009**.
[14] M. Dumortier, S. Tembhurne, S. Haussener, *Energy Environ. Sci.* **2015**, *8*, 3614–3628.
[15] Q. Wang, T. Hisatomi, Q. Jia, H. Tokudome, M. Zhong, C. Wang, Z. Pan, T. Takata, M. Nakabayashi, N. Shibata, Y. Li, I. D. Sharp, A. Kudo, T. Yamada, K. Domen, *Nat. Mater.* **2016**, *15*, 611–615.
[16] D. M. Fabian, S. Hu, N. Singh, F. A. Houle, T. Hisatomi, K. Domen, F. E. Osterloh, S. Ardo, *Energy Environ. Sci.* **2015**, *8*, 2825–2850.
[17] K. Fujihara, T. Ohno, M. Matsumura, *J. Chem. Soc. Faraday Trans.* **1998**, *94*, 3705–3709.
[18] R. Abe, K. Sayama, K. Domen, H. Arakawa, *Chem. Phys. Lett.* **2001**, *344*, 339–344.
[19] R. Abe, K. Sayama, H. Sugihara, *J. Phys. Chem. B* **2005**, *109*, 16052–16061.
[20] K. Tennakone, R. Tantrigoda, S. Abeysinghe, S. Punchihewa, C. A. N. Fernando, *J. Photochem. Photobiol. A* **1990**, *52*, 43–46.
[21] G. N. Schrauzer, T. D. Guth, *J. Am. Chem. Soc.* **1977**, *99*, 7189–7193.
[22] H. Van Damme, W. K. Hall, *J. Am. Chem. Soc.* **1979**, *101*, 4373–4374.
[23] T. Kawai, T. Sakata, *Chem. Phys. Lett.* **1980**, *72*, 87–89.
[24] R. Asai, H. Nemoto, Q. Jia, K. Saito, A. Iwase, A. Kudo, *Chem. Commun.* **2014**, *50*, 2543–2546.
[25] Y. Sasaki, H. Nemoto, K. Saito, A. Kudo, *J. Phys. Chem. C* **2009**, *113*, 17536–17542.
[26] K. Sayama, R. Yoshida, H. Kusama, K. Okabe, Y. Abe, H. Arakawa, *Chem. Phys. Lett.* **1997**, *277*, 387–391.
[27] K. Sayama, K. Mukasa, R. Abe, Y. Abe, H. Arakawa, *Chem. Commun.* **2001**, 2416–2417.
[28] K. Maeda, M. Higashi, D. Lu, R. Abe, K. Domen, *J. Am. Chem. Soc.* **2010**, *132*, 5858–5868.
[29] K. Maeda, D. Lu, K. Domen, *Chem. Eur. J.* **2013**, *19*, 4986–4991.
[30] M. Higashi, R. Abe, A. Ishikawa, T. Takata, B. Ohtani, K. Domen, *Chem. Lett.* **2008**, *37*, 138–139.
[31] M. Hara, T. Kondo, M. Komoda, S. Ikeda, J. N. Kondo, K. Domen, M. Hara, K. Shinohara, A. Tanaka, *Chem. Commun.* **1998**, 357–358.
[32] L. Liao, Q. Zhang, Z. Su, Z. Zhao, Y. Wang, Y. Li, X. Lu, D. Wei, G. Feng, Q. Yu, X. Cai, J. Zhao, Z. Ren, H. Fang, F. Robles-Hernandez, S. Baldelli, J. Bao, *Nat. Nanotechnol.* **2014**, *9*, 69–73.
[33] S. Hu, C.-Y. Chi, K. T. Fountaine, M. Yao, H. A. Atwater, P. D. Dapkus, N. S. Lewis, C. Zhou, *Energy Environ. Sci.* **2013**, *6*, 1879–1890.
[34] J. Xu, C. Pan, T. Takata, K. Domen, *Chem. Commun.* **2015**, *51*, 7191–7194.
[35] C. Pan, T. Takata, M. Nakabayashi, T. Matsumoto, N. Shibata, Y. Ikuhara, K. Domen, *Angew. Chem. Int. Ed.* **2015**, *54*, 2955–2959; *Angew. Chem.* **2015**, *127*, 2998–3002.
[36] A. E. Maegli, E. H. Otal, T. Hisatomi, S. Yoon, C. M. Leroy, N. Schäuble, Y. Lu, M. Grätzel, A. Weidenkaff, *Energy Procedia* **2012**, *22*, 61–66.
[37] R. Abe, T. Takata, H. Sugihara, K. Domen, *Chem. Commun.* **2005**, 3829–3831.

[38] R. Liu, L. H. Han, Z. Q. Huang, I. M. Ferrer, A. H. M. Smets, M. Zeman, B. S. Brunschwig, N. S. Lewis, *Thin Solid Films* **2015**, *586*, 28 – 34.
[39] S. S. K. Ma, K. Maeda, T. Hisatomi, M. Tabata, A. Kudo, K. Domen, *Chem. Eur. J.* **2013**, *19*, 7480 – 7486.
[40] K. Maeda, K. Teramura, D. Lu, T. Takata, N. Saito, Y. Inoue, K. Domen, *Nature* **2006**, *440*, 295.
[41] J. Sato, N. Saito, Y. Yamada, K. Maeda, T. Takata, J. N. Kondo, M. Hara, H. Kobayashi, K. Domen, Y. Inoue, *J. Am. Chem. Soc.* **2005**, *127*, 4150 – 4151.
[42] K. Maeda, T. Takata, M. Hara, N. Saito, Y. Inoue, H. Kobayashi, K. Domen, *J. Am. Chem. Soc.* **2005**, *127*, 8286 – 8287.
[43] Y. Lee, H. Terashima, Y. Shimodaira, K. Teramura, M. Hara, H. Kobayashi, K. Domen, M. Yashima, *J. Phys. Chem. C* **2007**, *111*, 1042 – 1048.
[44] Z. Zou, J. Ye, K. Sayama, H. Arakawa, *Nature* **2001**, *414*, 625 – 627.
[45] Z. Zou, H. Arakawa, *J. Photochem. Photobiol. A* **2003**, *158*, 145 – 162.
[46] Z. H. Pan, T. Hisatomi, Q. Wang, S. S. Chen, M. Nakabayashi, N. Shibata, C. S. Pan, T. Takata, M. Katayama, T. Minegishi, A. Kudo, K. Domen, *ACS Catal.* **2016**, *6*, 7188 – 7196.
[47] E. Verlage, S. Hu, R. Liu, R. J. R. Jones, K. Sun, C. Xiang, N. S. Lewis, H. A. Atwater, *Energy Environ. Sci.* **2015**, *8*, 3166 – 3172.
[48] J. R. McKone, B. F. Sadtler, C. A. Werlang, N. S. Lewis, H. B. Gray, *ACS Catal.* **2013**, *3*, 166 – 169.
[49] M. Liu, W. You, Z. Lei, G. Zhou, J. Yang, G. Wu, G. Ma, G. Luan, T. Takata, M. Hara, K. Domen, C. Li, *Chem. Commun.* **2004**, 2192 – 2193.
[50] K. Sayama, R. Abe, H. Arakawa, H. Sugihara, *Catal. Commun.* **2006**, *7*, 96 – 99.
[51] Y. Sasaki, H. Kato, A. Kudo, *J. Am. Chem. Soc.* **2013**, *135*, 5441 – 5449.
[52] D. Tromans, *Hydrometallurgy* **1998**, *48*, 327 – 342.
[53] J. H. Carpenter, *Limnol. Oceanogr.* **1966**, *11*, 264 – 277.
[54] M. Geng, Z. Duan, *Geochim. Cosmochim. Acta* **2010**, *74*, 5631 – 5640.
[55] R. F. Weiss, *Deep Sea Res. Oceanogr. Abstr.* **1970**, *17*, 721 – 735.
[56] M. Görgényi, J. Dewulf, H. Van Langenhove, K. Héberger, *Chemosphere* **2006**, *65*, 802 – 810.
[57] A. Schumpe, I. Adler, W. D. Deckwer, *Biotechnol. Bioeng.* **1978**, *20*, 145 – 150.
[58] E. Green, D. Carritt, *J. Mar. Res.* **1967**, *25*, 140 – 147.
[59] M. L. Hitchman, *Measurement of Dissolved Oxygen*, Wiley, New York, **1978**.
[60] E. W. Lard, R. C. Horn, *Anal. Chem.* **1960**, *32*, 878 – 879.
[61] P. R. Haddad in *Handbook on Metals in Clinical and Analytical Chemistry* (Eds.: H. Seiler, A. Sigel, H. Sigel), Marcel Dekker, Inc., New York **1994**, pp. 135 – 148.
[62] J. Colaruotolo, R. Eddy, *Anal. Chem.* **1977**, *49*, 884 – 885.
[63] Y. Noguchi, L. Zhang, T. Maruta, T. Yamane, N. Kiba, *Anal. Chim. Acta* **2009**, *640*, 106 – 109.
[64] B. Szostek, J. Orska-Gawrys, I. Surowiec, M. Trojanowicz, *J. Chromatogr. A* **2003**, *1012*, 179 – 192.
[65] S. Schnell, S. Ratering, K.-H. Jansen, *Environ. Sci. Technol.* **1998**, *32*, 1530 – 1537.
[66] M. E. Aliaga, C. Carrasco-Pozo, C. López-Alarcón, C. Olea-Azar, H. Speisky, *Bioorg. Med. Chem.* **2011**, *19*, 534 – 541.
[67] G. Peintler, A. Nagy, A. K. Horvath, T. Kortvelyesi, I. Nagypal, *Phys. Chem. Chem. Phys.* **2000**, *2*, 2575 – 2586.

Manuscript received: December 27, 2016
Revised: January 30, 2017
Accepted Article published: January 30, 2017
Final Article published: March 16, 2017